

# A 4D sedimentological approach to reconstructing the flood frequency and intensity of the Rhône River (Lake Bourget, NW European Alps)

J.-P. Jenny · B. Wilhelm · F. Arnaud ·  
P. Sabatier · C. Giguet Covex · A. Mélo ·  
B. Fanget · E. Malet · E. Ployon · M. E. Perga

Received: 28 January 2013 / Accepted: 20 January 2014 / Published online: 7 February 2014  
© Springer Science+Business Media Dordrecht 2014

**Abstract** A high-resolution sedimentological study of Lake Bourget was conducted to reconstruct the flood frequency and intensity (or magnitude) in the area over the last 350 years. Particular emphasis was placed on investigating the spatio-temporal distribution of flood deposits in this large lake basin. The thicknesses of deposits resulting from 30 flood events of the Rhône River were collected over a set of 24 short sediment cores. Deposit thicknesses were compared with instrumental data for the Rhône River discharge for the period from 1853 to 2010. The results show that flood frequency and intensity cannot be

reliably reconstructed from a single core because of the inhomogeneous flood-deposit geometry in such a large lake. From all documented flood-deposit thicknesses, volumes of sediment brought into the lake during each flood event were computed through a Kriging procedure and compared with the historical instrumental data. The results show, in this study, that reconstructed sediment volumes are well correlated to maximal flood discharges. This significant correlation suggests that the increase of embankment and dam settlements on the Rhône River during the last 150 years has not significantly affected the transport of the smallest sediment fraction during major flood

---

J.-P. Jenny (✉) · B. Wilhelm · F. Arnaud ·  
P. Sabatier · C. Giguet Covex · A. Mélo ·  
B. Fanget · E. Malet · E. Ployon  
Edytem, CNRS, Université de Savoie,  
73376 Le Bourget du Lac Cedex, France  
e-mail: jean-philippe.jenny@univ-savoie.fr

B. Wilhelm  
e-mail: wilhelm@unice.fr

F. Arnaud  
e-mail: fabien.arnaud@univ-savoie.fr

P. Sabatier  
e-mail: pierre.sabatier@univ-savoie.fr

C. Giguet Covex  
e-mail: Charline.Giguet-Covex@univ-savoie.fr

A. Mélo  
e-mail: melo.alain@wanadoo.fr

B. Fanget  
e-mail: bernard.fanget@univ-savoie.fr

E. Malet  
e-mail: emmanuel.malet@univ-savoie.fr

J.-P. Jenny · M. E. Perga  
INRA, UMR CARRTEL, Université de Savoie,  
74203 Thonon-les-bains Cedex, France  
e-mail: perga@thonon.inra.fr

B. Wilhelm  
Géoazur, CNRS, IRD, OCA, Université de Nice  
Sophia-Antipolis, 06560 Valbonne, France

C. Giguet Covex  
Laboratoire d'Ecologie Alpine, CNRS, Université Joseph  
Fourier, 38041 Grenoble Cedex 9, France

events. Hence, assessment of the flood-sediment volumes deposited in the large Lake Bourget is the only way to reliably reconstruct the flood frequency and intensity.

**Keywords** Flood intensity and frequency · Sediment distribution · Fluvial discharge · Human activity

## Introduction

Floods of large European rivers are some of the most significant natural hazards, causing serious human and economic losses (Münich Re Group 2003). Currently, the current global warming trend is expected to lead to an intensification of the hydrological cycle, which could result in an increase in the frequency and intensity (or magnitude) of extreme precipitations events (Allen and Ingram 2002; IPCC et al. 2007). This could result in an increasing flood hazard within the next decades (Christensen and Christensen 2003; Trenberth and Dai 2007). A reliable assessment of the future evolution of flood events thus becomes a crucial issue. However, the stochastic nature and the rare occurrence of these events make it difficult to identify trends based on instrumental data alone (Frei and Schär 2001). To overcome these limits, the study of lake sediments can provide flood records long enough to identify the natural variability of the flood activity over a wide-ranging frequency spectrum (Czymzik et al. 2010; Wilhelm et al. 2012a) and, thereby making it possible to understand the physical processes driving the flood occurrence and intensity throughout various global climate states.

Paleolimnological studies have shown that the past evolution of flood frequency can be reliably assessed from the identification and the dating of flood deposits (Czymzik et al. 2010; Ito et al. 2010; Schiefer et al. 2011; Giguet-Covex et al. 2012; Gilli et al. 2003, 2013). However, in the case of large lakes, the incoming river-flow may develop meandering channel systems and distal basin fan lobes (Mulder and Chapron 2011) or river plume deviation (Girardclos et al. 2003), resulting in a high spatial heterogeneity of the flood deposits over large lake basins and biasing flood reconstructions when a unique core is studied. Through a high-resolution spatial approach, we aim thus at assessing the distribution of the flood deposits in

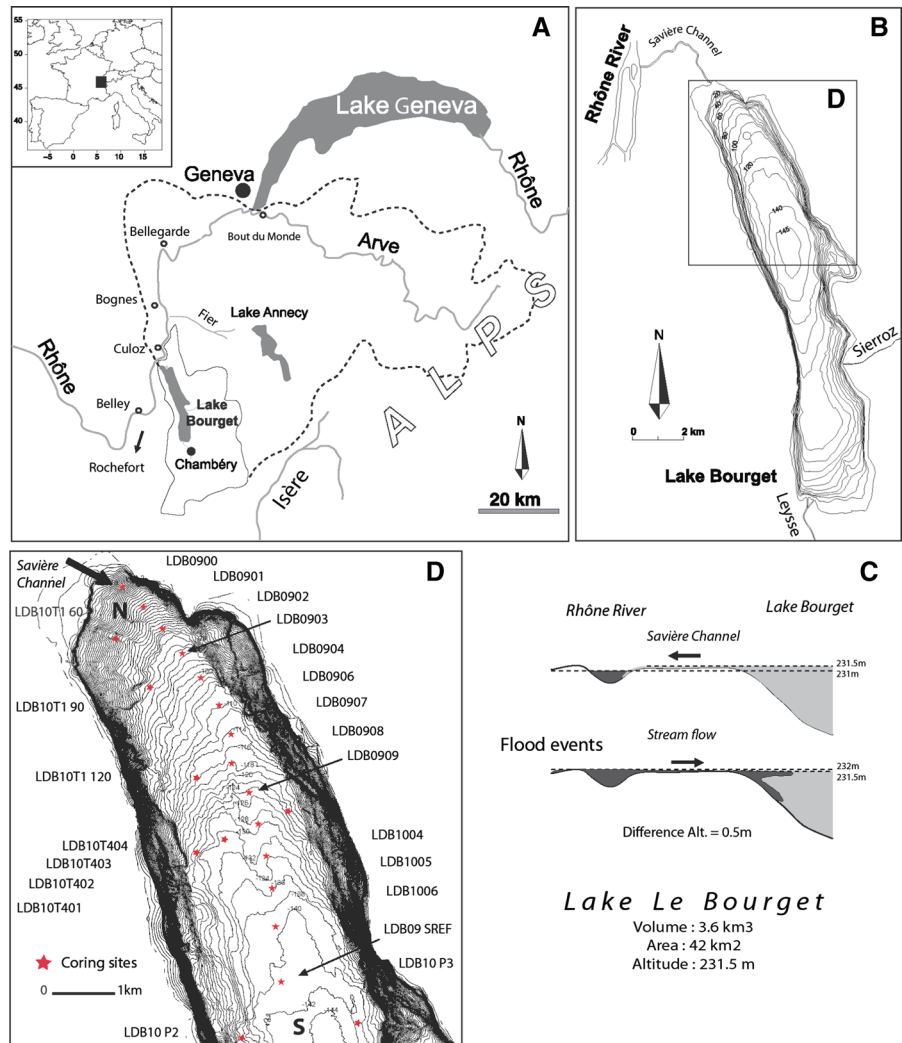
a large lake to test the reliability of the flood frequency reconstructed from a single core as is classically done.

Past changes in flood intensity are even more difficult to assess. In a few cases, intensities were assessed from the grain size (Lapointe et al. 2012; Wilhelm et al. 2012a, 2013; Giguet-Covex et al. 2012), which is assumed to represent the river energy and, thereby, the discharge (Campbell 1998; Mulder et al. 2001). Intensities were also assessed from the thickness of the flood deposit (Schiefer et al. 2011; Wilhelm et al. 2012b), which is assumed to represent the total amount of sediment transported and deposited during the flood event. This latter method seems to require a homogeneous spatial distribution of flood deposits (Schiefer et al. 2011; Wilhelm et al. 2012b). Through a high-resolution spatial approach, we aim at testing the reliability of the flood intensity reconstruction in a large lake from flood thicknesses or from estimates of sediment volumes transported and deposited during a flood. We chose Lake Bourget, whose dimensions were well suited to a large spatial investigation, because flood deposits for this lake had been previously documented (Arnaud et al. 2005, 2012; Chapron et al. 2005; Debret et al. 2010) and characterised (Chapron et al. 2002; Revel-Rolland et al. 2005). Finally, anthropogenic settlement history (dams and embankments) was compared with the reconstruction of the flood regime to discuss the relationships between changes in the flood regime, climate, and human settlements.

## Study site and settings

Lake Bourget (231.5 m asl, 147 m deep, 18 km long, and 2.8 km wide) is a narrow over-deepened hard-water lake at the northwestern edge of the French Alps (Fig. 1a). The small Lysse and Sierroz Rivers usually feed the Lake Bourget waters, which then flow to the Rhône River by the Savière channel (Fig. 1b). However, during severe flooding of the Rhône River, the water-current of this channel is reversed, most of waters pass also through the Chautagne swamps (as observed for 1990 flood event), and waters of the Rhône River enter then into Lake Bourget (Fig. 1c). During such flood events, the Lake Bourget catchment area is 4,600 km<sup>2</sup>, including tributaries draining part of the Jura Mountains and the Inner Alps. The Rhône River provides predominantly illite and reworked particles transported by the Arve River that were

**Fig. 1** **a** Location map and catchment area of Lake Bourget. **b** Main tributaries (Rhône, Leyss, and Sieroz River) and effluent (Rhône River) of Lake Bourget. **c** The Savière channel generally flows from Lake Bourget to the Rhône River; however, the flow is reversed during severe flooding of the Rhône River. **d** Bathymetry and core locations in the North area



eroded by glaciers in the Mont-Blanc External Crystalline massifs (Revel-Rolland et al. 2005; Debret et al. 2010). Previous studies showed that sediments of the northern lake area are composed of autochthonous and allochthonous sediments (Arnaud et al. 2005, 2012; Giguet-Covex et al. 2010). The allochthonous fraction is generally mixed with the autochthonous fraction (between 10 and 40 % of the bulk sediment) but can also generate individual deposits during high-energy flood events. The grain size of the terrigenous fraction is almost constant over the whole Holocene whether it is diluted in the autochthonous matrix or sampled in individual flood deposits (Arnaud et al. 2005). The grain size is characterised by a mode ranging from 6 to 9  $\mu\text{m}$ , precluding the use of grain size as a marker of intensity.

Rhône River settlements

The natural braided-shape system of the Rhône River was modified by human settlements during the second part of the 1700s (Fig. 2). Since AD 1774, the left riverbank has been protected by discontinuous embankments that reduce overflowing and the transport of sediments into the Chautagne swamps. In the second part of the 1800s, both the left and right sides of the river were embanked, leading to the current linear configuration of the Rhône, which is well suited for navigation and commerce. The construction of the first hydropower dams around AD 1900 (Chèvres in 1896; Giffre in 1897; Chadde in 1896, Val de Fier in AD 1909) on the Rhône River and on its major tributaries (Giffre, Arve and Fier) increased the retention of

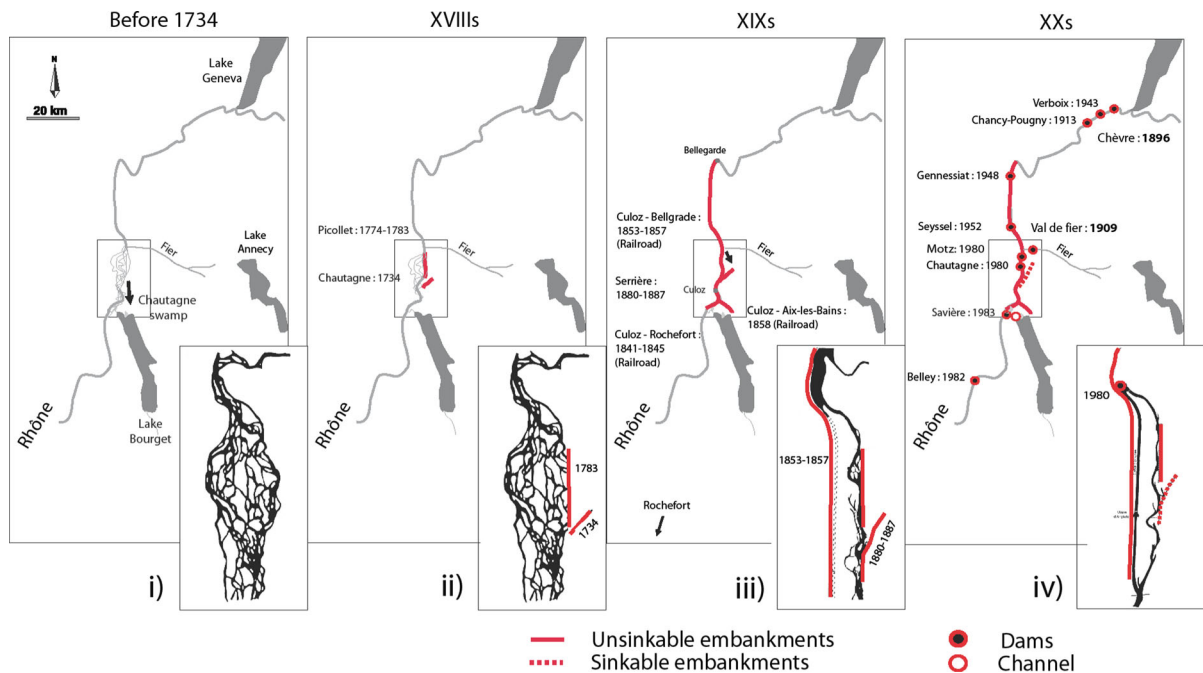


**Fig. 2** Historical human settlements and corresponding morphology of the upper Rhône River from 1734 to 2009. The 1700s and 1800s are characterised by an increase in embankments, whereas the 1900s were mainly affected by dams

sediments from the main source contributors (Giuliani et al. 1994; Viollet 2005). Finally, since AD 1913, seven additional dams (hydropower and impoundments) have been constructed along the Rhône River and regulate the discharge between Geneva and Lake Bourget (Fig. 2). Between the Rhône River and Lake Bourget, the Savière channel underwent settlements over time (e.g., channelized during the 1900s) but may not have altered the sediment transport regime during high flood events. Indeed, during highest intensity flood events, only a small proportion of the water flows throughout the Savière into the lake as compared to the water that overflows from the Rhône course above the Chautagne swamp (as observed in 1990 AD).

## Materials and methods

### Coring sites

The high-resolution spatiality of the flood deposition was assessed through 24 short cores sampled from the northern area of the lake using a gravity corer (Uwitec Ltd., Austria). Coring sites were selected along a proximal-distal transect from the Savières channel to

the deep basin and along a transversal transect, cross-cutting the proximal-distal transect at its halfway point (Fig. 1c). Five additional cores were taken at the side of transects to limit spatial gaps.

### Age model

Previous studies of recent sediments from the deep basin offer clearly identifiable chronological markers for dating. Giguet-Covex et al. (2010) have indeed shown that the most superficial sediment has been made up of biochemical varves since at least the 1940s. More-recent studies revealed that these varve facies started in 1933 in the deepest part of the lake and reached half the total lake area in the 1950s (Jenny et al. 2013). In addition, three particular deposits were identified as resulting from the catastrophic floods of the Rhône River in AD 1711 and 1733 (Champion 1839), and from the earthquake of Chautagne in AD 1822 (Chapron et al. 1999). Based on these chronological markers, individual sedimentation rates were calculated for five cores (LDB0904, LDB0906, LDB1005, LDB1006, LDB10SREF) that were selected because of their position along the proximal-distal transect and the visual identification of the

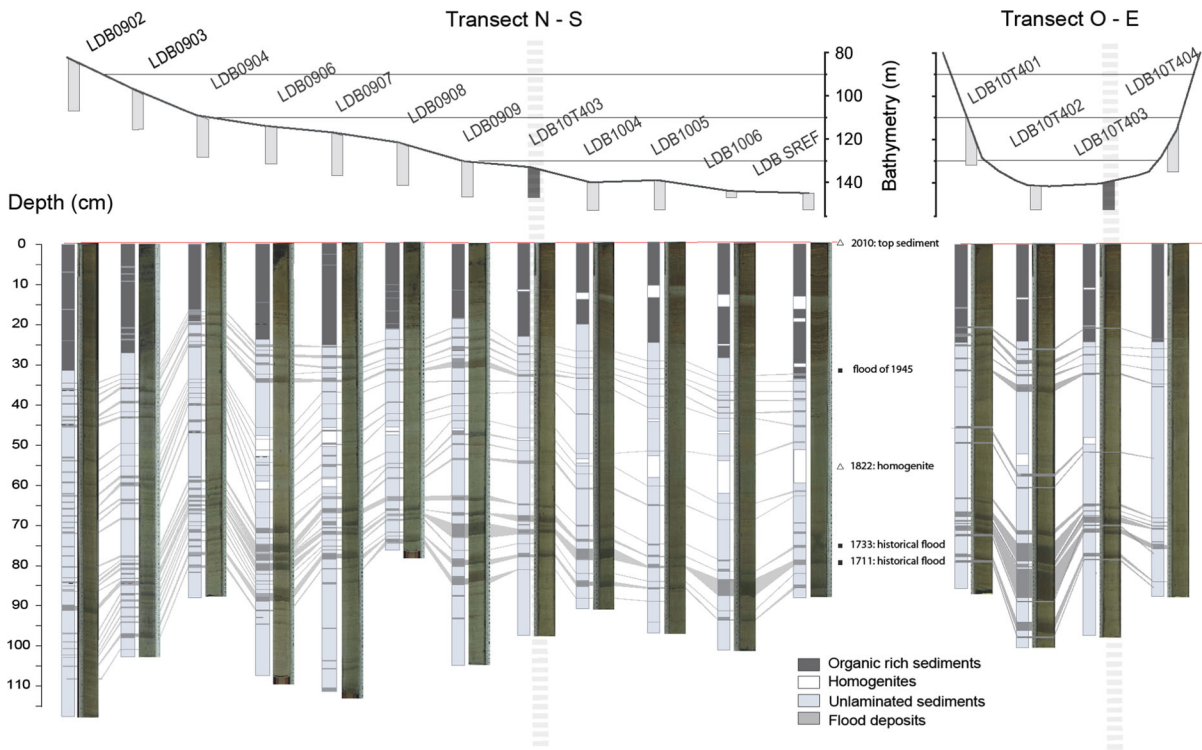


**Fig. 3** Correlation of flood events between cores of longitudinal and transversal transects. Five lithostratigraphics markers corresponded to well-documented historical events (1711, 1733, 1822, 1945, and 2010)

above-mentioned tie points (Jenny et al. 2013). Ages of all flood deposits were calculated by interpolation of the sedimentation rates. Then, a synthetic depth-to-age model was computed from the five individual models and adjusted on dates of historical flood events to reduce dating uncertainties. The other 17 cores were dated by stratigraphic correlations (Fig. 3).

**Modelling flood deposits: spatial distribution and volumetric assessment**

Flood deposit thicknesses were documented for all cores on fresh sediment and from high-resolution digital images (3,500 dpm). Two-dimensional modelling of geometrical extensions of flood deposits was performed for each recorded flood event using the gridding and contour mapping software SURFER 9. Different gridding models were used to interpolate the extensions of flood deposits between core locations. The natural neighbourhood affected by an anisotropic ratio of 2 was chosen to generate an axial-flow direction of the sediment distribution.

The volumes of flood sediments were then computed by interpolation of the deposit thicknesses. The uncertainties in the estimated volumes were calculated by taking into consideration the standard deviation of the calculated volumes for the different interpolation methods. Volumes were calculated for seven different core datasets: (1) the first took into account all 24 cores, (2) five others used the 3, 4, 5, 6, and 7 most distal cores sampled from the deep basin, and (3) the seventh used the 6 most proximal cores sampled close to the river mouth. These calculations were performed to estimate the preferential zones of flood-sediment accumulation and the representativeness of reconstructions based on all cores compared with reconstructions based on cores from the proximal or distal areas only.

**Validation of reconstruction using monitoring and historical data**

To assess the reliability of the flood record, it was first compared with an exceptional long-term monitoring

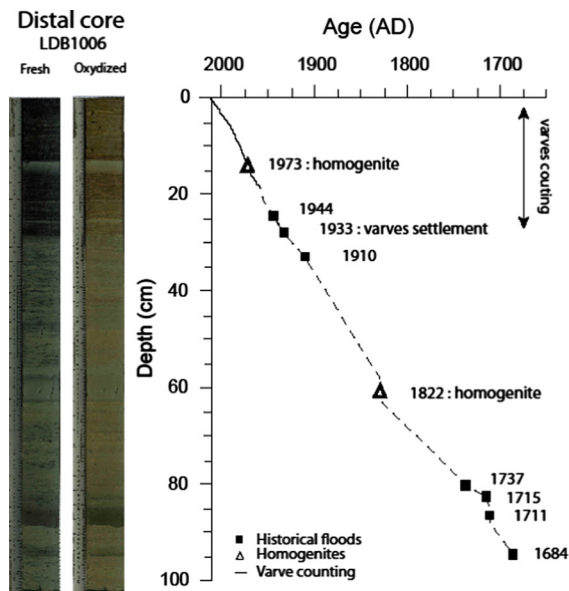


**Fig. 4** Age depth model of distal core LDB1006 from varve counting, radionuclides ( $^{10}\text{Pb}$ ,  $^{137}\text{Cs}$ , and  $^{241}\text{Am}$ ) (Jenny et al. 2013) and historical events (floods and 1822 homogenite). Ages were interpolated between dated lithological markers

series from the Rhône River (CEMAGREF 2000). The maximum annual discharges of the Rhône River were calculated from water levels measured at the Bognes hydrological station (Fig. 1a) for the period from 1853 to 2000 (CEMAGREF 2000). Discharges from two recent major flood events (2002, 2004) were measured by Compagnie National du Rhône (CNR) and included to complete the sequence to the present day. To extend the instrumental record, historic flood dates of the Rhône and Arve Rivers were compiled from historical books and reviews back to 1650 AD (Champion 1839; Pardé 1928; Bravard 1987).

## Results

### Identification and dating of flood deposits

A total of 30 deposits of flood events and the chronological markers were identified and correlated (Fig. 3). An age-depth model is presented for the distal core LDB1006 (Fig. 4). Based on the varve counting and the clearly identifiable chronological markers of AD 1711, 1733, and 1822, mean sedimentation rates were obtained:  $0.23 \pm 0.04$ ,  $0.20 \pm 0.04$ ,  $0.24 \pm 0.04$ ,  $0.23 \pm 0.04$ , and  $0.24 \pm 0.04$   $\text{cm y}^{-1}$  for cores

LDB0904, LDB0906, LDB1005, LDB1006, and LDB10SREF, respectively. These sedimentation rates provided the five models used to date all 30 flood deposits (Fig. 5). A mean dispersion of  $7 \pm 3$  years appeared between the ages of flood deposits triggered by a common event. Except when the ages of flood deposits were in agreement with historic flood dates of the Rhône and Arve Rivers (black triangles, Fig. 5), the mean ages of each flood deposit were retained for the remainder of the study. Hence, the mean sedimentation rate and historic data provided a synthetic model represented by black squares in Fig. 5.

### Spatio-temporal distribution of flood deposits

To assess the distribution of the flood deposits through time and space, in Fig. 6, we represent a complete overview of the 30 flood deposits, together with their thickness, along the longitudinal and transversal transects. Cores located in the deep basin (LDB10T403, LDB1004, LDB1005, LDB1006, and LDB10SREF) recorded only (on average) 35 % of all the 30 inventoried flood deposits. In contrast, the closer the cores are to the delta (LDB10T1-120, LDB0906, LDB0904, LDB0903, and LDB0902), the more exhaustively they record the flood events (80, 73, 90, 97, and 93 %, respectively). Thinner deposits (2–4 mm) were identified in cores from the proximal zone, while thicker deposits were observed in the distal zone (2–70 mm). These results suggest that cores of the proximal zone are more suitable for reconstruction of the flood frequency and that cores from the distal zone could be more suitable for reconstruction of the flood intensity in the case of an approach based on the flood-deposit thickness. Distributions over the transversal transect show that the thickest flood deposits were mostly recorded in the deepest zone (core LDB10T402). Moreover, flood sediments seem to be deposited more often in the western part (LDB10T401) than in the eastern part (LDB10T404) of the basin.

The spatial distribution of flood deposits can be investigated through a modelling map (Fig. 7). Figure 7a presents the spatial distribution of seven contrasted flood deposits, ranked from the lowest to the highest volumes. Events with the lowest flood-sediment volumes only cover the proximal zone, whereas events with the highest volumes spread from the proximal zone to the deep basin (Fig. 7b). This

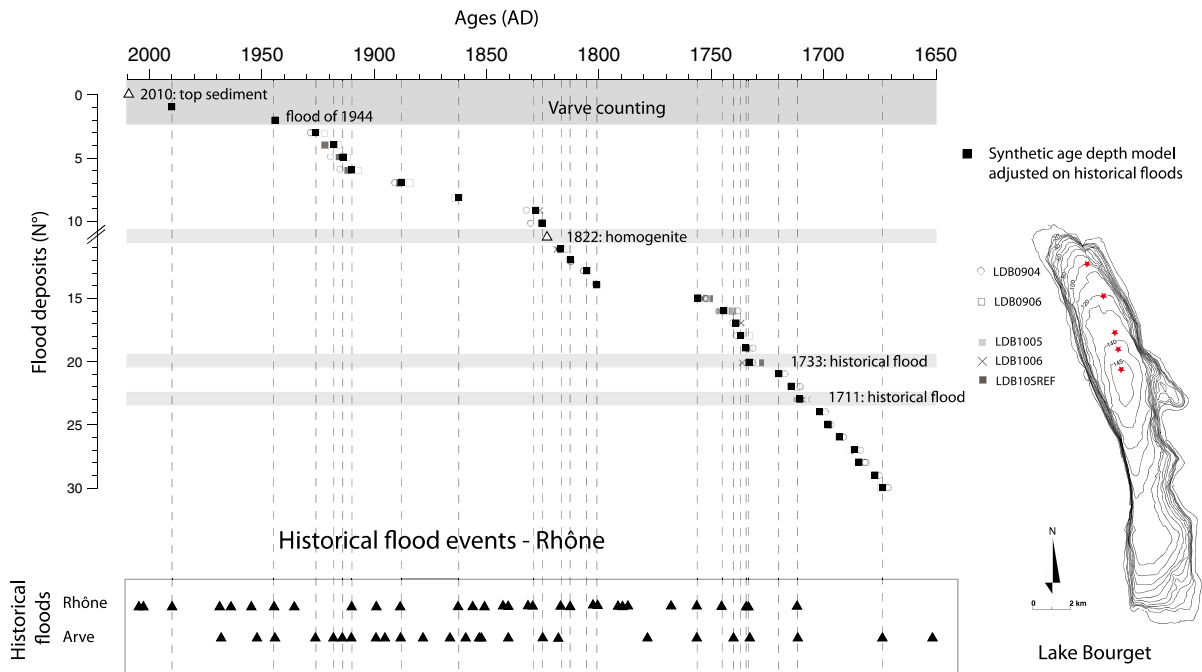


**Fig. 5** Flood event dating according to five independent age depth models calculated from varve counting and from five well-documented historical events (1711, 1733, 1822, 1945, and

2010). A synthetic model (*black squares*) was adjusted based on the closest historical flood events of the Rhône and Arve Rivers

confirms the intuitive statement that during a given flood event, the higher the volume of transported sediments, the more distal the deposit accumulation. As a consequence, there is a link between the velocity of the incoming current and the total deposited volume of sediment. Furthermore, the mapping reveals various changing and complex pathways of hyperpycnal flows from one event to another, indicating that flood sediments are highly heterogeneously distributed in the whole basin. This suggests that only flood reconstructions based on a multi-core assessment of flood-sediment volumes could reliably reconstruct the flood frequency and intensity in large lakes.

To verify the representativeness of each core flood-deposit record, we reported the records of flood frequency and flood intensity for each individual core ( $\times 24$  cores) and for multiple-core assemblages of the distal, proximal, and total area (Table 1). The records were systematically correlated to the total reconstruction, which means that the total reconstruction—presented in the bottom panel—corresponds to the best reproduction of flood frequency (100 % reproduced) and intensities ( $r^2 = 1.00$ ,  $p < 0.001$ ). For instance, core LDB0902 records 93 % of the flood

events, corresponding to a good reproduction of frequency, but to a relatively poor reconstruction of intensity ( $r = 0.45$ ,  $p > 0.01$ ). More generally, Table 1 highlights the fact that cores from the distal zone reproduce the flood frequency poorly (mean  $35 \pm 20$  %) but reproduce the flood intensity quite well (mean  $r = 0.81 \pm 0.01$ ). In contrast, sequences of proximal cores reproduce the flood frequency well (mean  $76 \pm 20$  %) but generally do not reproduce intensity (mean  $r = 0.5 \pm 0.01$ ).

In Table 1, reconstructions based on multiple-core assemblages, both from the proximal (one set of 6 cores) and the distal areas (five sets of 3, 4, 5, 6, and 7 cores) were also compared with the total reconstruction (Table 1, bottom panel). The best combination to reproduce the flood frequency is the assemblage from multiple proximal cores (100 % frequency reproduced). Assemblages from the distal zone reproduced 47–67 % of the total frequency, which is much better than the reconstruction obtained from isolated cores (mean  $35 \pm 20$  %). However, the intensity is well reproduced by assemblages from the distal zone (mean  $r = 0.92 \pm 0.15$ ,  $p < 0.001$ ), but by none of the assemblages from the proximal zone (the only

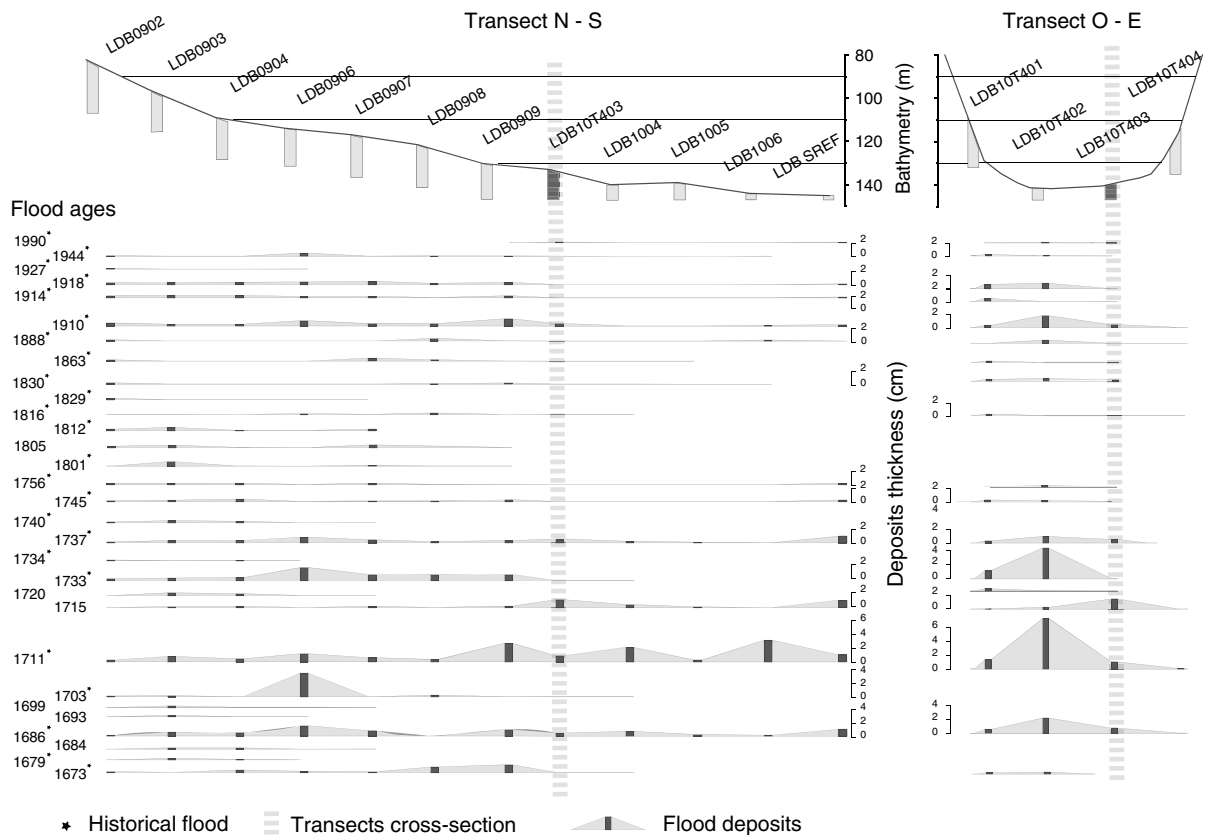


**Fig. 6** Spatio-temporal distribution of flood deposits along the longitudinal and transversal transects. Core LDB10T403 corresponds to the cross section between the two transects.

The ages of flood events are plotted on the *left side*. *Black stars* indicate flood deposits related to referenced historical events

example is from the 6-core reconstruction with  $r = 0.55$ ,  $p < 0.01$ ).

Finally, all the reconstructions of flood intensity were compared with the monitored maximum annual discharge for the period from 1853 to 2004 (Table 1, right side). The correlations are significant only for the reconstruction from multiple-core assemblages of the distal zone (7 cores,  $r = 0.93$ ,  $p < 0.001$ ) and the total reconstruction (24 cores,  $r = 0.90$ ,  $p < 0.001$ ).

## Discussion

### Sediment supplies, remobilisation, and deposition

Attempting the reconstruction of past flood regime from sediment archives necessitates first an overview of lake sedimentation processes leading to such archive formation: sediment supplies, remobilisation, and deposition.

During flood events, Lake Bourget is supplied by sediments from the Rhône and the Arve Rivers. The length of the main upstream tributary (Rhône and Arve Rivers) is about 250 km. Hence we can assume that such a long distance may have prevented the limitation in sediment supplies during flood events, more specifically because the source of the Arve River constitutes a mountain massif where exposed rocks can be more easily eroded. This hypothesis of a non-limitation in particle supplies is confirmed by the record of several huge volumes of allocthonous sediments deposited during highest intensity flood events ( $>10^3 \text{ m}^3$  in the 1900s;  $>50^3 \text{ m}^3$  in the 1700s). Indeed, in sediment cores, the short return period of these events, in the early 1700s (e.g., 1711, 1715, 1720, 1733) or in the early 1900s (1910, 1914, 1918, 1927), highlights that even after a high intensity flood event it is still possible for the following one to transport large volumes of sediments to the lake. The preservation of all inventoried historical floods (during

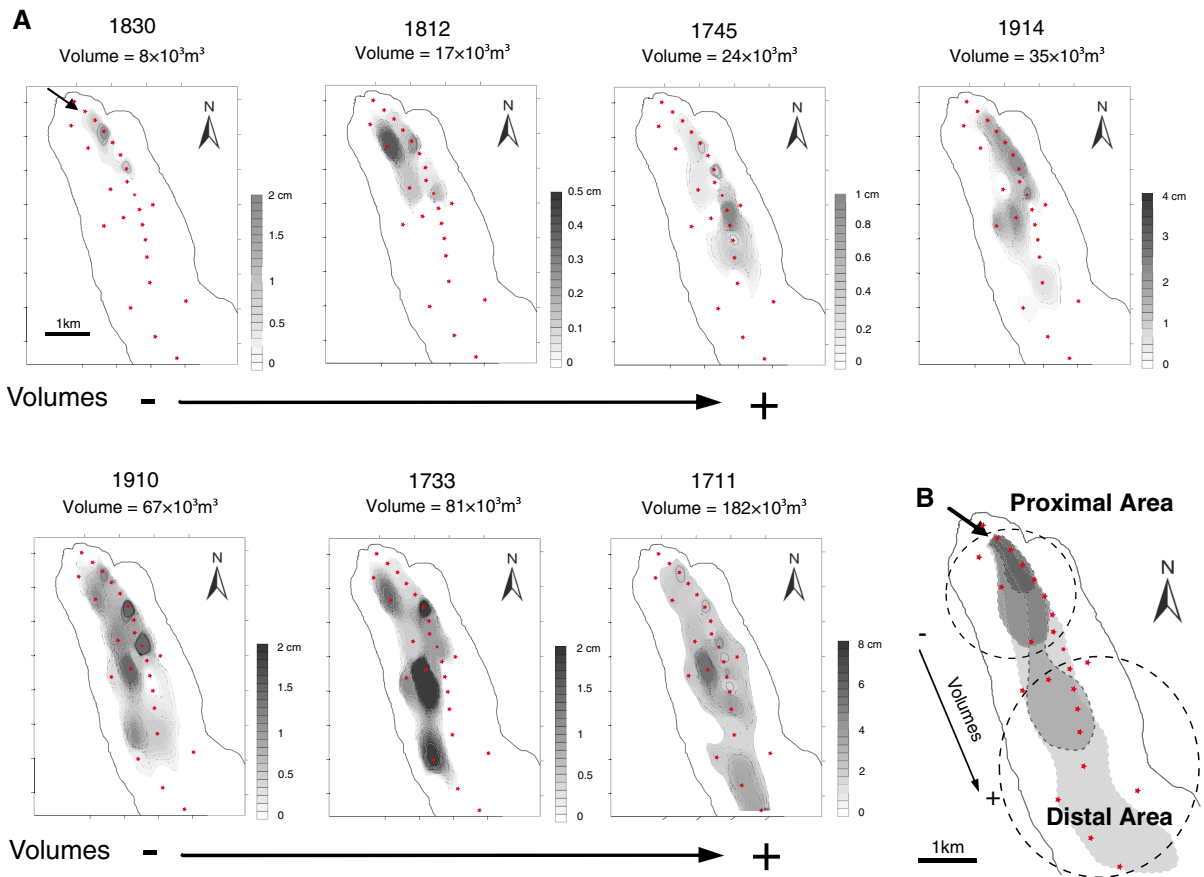


**Fig. 7** **a** Spatial thickness distribution of flood sediments for seven selected events, ranked from low volumes (left top) to higher volumes (right bottom). **b** Conception scheme of flood-triggered sediment distribution, according to volumes of

sediments brought into the lake during floods. The greater the sediments volume, the more distal the distribution. The meandering distribution is also arbitrarily schematised

phases of short flood return period) also highlights that flood deposits were not eroded by the close following event. This characteristic ensures the good preservation of a complete flood sequence in the record. Hence external sedimentological conditions (supplies and remobilisations) seem appropriate to the record of a representative flood regime signal by lake sediment archives.

In Lake Bourget, the spatial deposition of flood-triggered sediments layers is synthesised in Fig. 8. Chapron et al. (2005) showed that sporadic high flood events produced centimeter-thick fine-grained hyperpycnites in the deep basin. In this study we show that hyperpycnites dispersion pattern seems to be dependent on the total sediment volume brought in the lake (i.e., the flow energy) during floods. The sediment distribution along a proximal-to-distal section can be

resumed as follows: large volumes of sediments brought during floods generate rare but thick deposits in the distal zone; lower volumes however generate frequent but thinner deposits in the proximal zone (Fig. 8). Over the whole basin area, sediments deposition was shown to be heterogeneous and we conclude that it necessitates a spatial investigation to reconstruct flood regime.

#### Flood reconstruction versus instrumental data (1853–2010)

The maximum annual discharge of the Rhône River has been continuously monitored since 1853 (Fig. 9). It ranged between 900 and  $1,300 \text{ m}^3 \text{ s}^{-1}$  on average, but it exceeded  $1,500 \text{ m}^3 \text{ s}^{-1}$  during ten major flood events (CEMAGREF 2000). Nine of these ten major

**Table 1** Assessment of the flood frequency reconstruction (detected flood deposits) and the flood intensity reconstruction (flood sediment volume) from individual cores (top panel) and multiple cores (bottom panel)

| Proxy                          | Cores         |                |            | Frequency               |            | Intensity                                     |                            |                                                                 |          |                            |
|--------------------------------|---------------|----------------|------------|-------------------------|------------|-----------------------------------------------|----------------------------|-----------------------------------------------------------------|----------|----------------------------|
|                                |               |                |            | Detected flood deposits |            | Correlation with total flood-sediment volumes |                            | Correlation with monitored maximal annual discharge (1853–2010) |          |                            |
|                                | Name          | Number         | Zone       | Number                  | (%)        | <i>r</i>                                      | <i>p</i> value             | Number of deposits                                              | <i>r</i> | <i>p</i> value             |
| Thicknesses                    | LDB0902       | 1              | Proximal   | 28                      | <b>93</b>  | 0.45                                          | <i>p</i> > 0.01            | 9                                                               | 0.65     | <i>p</i> < 0.1             |
|                                | LDB0903       | 1              | Proximal   | 29                      | <b>97</b>  | 0.31                                          | <i>p</i> > 0.1             | 5                                                               | 0.95     | <i>p</i> < 0.1             |
|                                | LDB0904       | 1              | Proximal   | 27                      | <b>90</b>  | 0.16                                          | <i>p</i> > 0.1             | 5                                                               | 0.93     | <i>p</i> < 0.1             |
|                                | LDB0906       | 1              | Proximal   | 22                      | <b>73</b>  | 0.49                                          | <i>p</i> > 0.01            | 6                                                               | 0.16     | <i>p</i> > 0.1             |
|                                | LDB0907       | 1              | Proximal   | 20                      | <b>67</b>  | 0.67                                          | <i>p</i> > 0.01            | 5                                                               | 0.71     | <i>p</i> > 0.1             |
|                                | LDB0908       | 1              | Proximal   | 15                      | 50         | 0.09                                          | <i>p</i> > 0.1             | 5                                                               | 0.49     | <i>p</i> > 0.1             |
|                                | LDB0909       | 1              | Proximal   | 21                      | <b>70</b>  | 0.66                                          | <b><i>p</i> &lt; 0.01</b>  | 6                                                               | 0.30     | <i>p</i> > 0.1             |
|                                | LDB10T1 90 m  | 1              | Proximal   | 20                      | <b>67</b>  | 0.32                                          | <i>p</i> > 0.1             | 5                                                               | 0.52     | <i>p</i> > 0.1             |
|                                | B17           | 1              | Proximal   | 10                      | 33         | 0.57                                          | <i>p</i> > 0.01            | 4                                                               | 0.46     | <i>p</i> > 0.1             |
|                                | LDB10T1 120 m | 1              | Distal     | 24                      | <b>80</b>  | 0.82                                          | <b><i>p</i> &lt; 0.001</b> | 6                                                               | 0.67     | <i>p</i> > 0.1             |
|                                | LDB10T403     | 1              | Distal     | 13                      | 43         | 0.86                                          | <i>p</i> > 0.01            | 2                                                               |          |                            |
|                                | LDB10T401     | 1              | Distal     | 17                      | 57         | 0.85                                          | <i>p</i> < 0.01            | 6                                                               | 0.86     | <i>p</i> < 0.1             |
|                                | LDB10T402     | 1              | Distal     | 15                      | 50         | 0.94                                          | <b><i>p</i> &lt; 0.001</b> | 5                                                               | 0.48     | <i>p</i> > 0.1             |
|                                | LDB10T404     | 1              | Distal     | 6                       | 20         | 0.00                                          |                            | 1                                                               |          |                            |
|                                | LDB1004       | 1              | Distal     | 10                      | 33         | 0.89                                          | <i>p</i> > 0.01            | 1                                                               |          |                            |
|                                | LDB1005       | 1              | Distal     | 9                       | 30         | 0.88                                          | <i>p</i> > 0.01            | 2                                                               |          |                            |
|                                | LDB1006       | 1              | Distal     | 9                       | 30         | 0.93                                          | <b><i>p</i> &lt; 0.01</b>  | 3                                                               |          |                            |
|                                | LDB SREF      | 1              | Distal     | 11                      | 37         | 0.84                                          | <b><i>p</i> &lt; 0.001</b> | 5                                                               | 0.59     | <i>p</i> > 0.1             |
|                                | LDB10 P2      | 1              | Distal     | 5                       | 17         | 0.76                                          | <i>p</i> > 0.1             |                                                                 |          |                            |
|                                | BB10          | 1              | Distal     | 10                      | 33         | 0.54                                          | <i>p</i> > 0.1             | 3                                                               | 0.87     | <i>p</i> > 0.1             |
|                                | B15           | 1              | Distal     | 5                       | 17         | 0.00                                          |                            |                                                                 |          |                            |
|                                | B11a          | 1              | Distal     | 5                       | 17         | 0.76                                          | <i>p</i> > 0.1             | 2                                                               |          |                            |
|                                | B12           | 1              | Distal     | 5                       | 17         | 0.54                                          | <i>p</i> > 0.1             | 1                                                               |          |                            |
|                                | Volumes       | Combination p1 | <b>6</b>   | Proximal                | 30         | <b>100</b>                                    | 0.55                       | <b><i>p</i> &lt; 0.01</b>                                       | 8        | 0.65                       |
| Combination p2                 |               | <b>7</b>       | Distal     | 20                      | <b>67</b>  | 0.93                                          | <b><i>p</i> &lt; 0.001</b> | 7                                                               | 0.90     | <b><i>p</i> &lt; 0.01</b>  |
| Combination p3                 |               | 6              | Distal     | 17                      | 57         | 0.94                                          | <b><i>p</i> &lt; 0.001</b> | 6                                                               | 0.69     | <i>p</i> > 0.1             |
| Combination p4                 |               | 5              | Distal     | 15                      | 50         | 0.95                                          | <b><i>p</i> &lt; 0.001</b> | 5                                                               | 0.36     | <i>p</i> > 0.1             |
| Combination p5                 |               | 4              | Distal     | 14                      | 47         | 0.92                                          | <b><i>p</i> &lt; 0.001</b> | 5                                                               | 0.52     | <i>p</i> > 0.1             |
| Combination p6                 |               | 3              | Distal     | 14                      | 47         | 0.87                                          | <b><i>p</i> &lt; 0.001</b> | 5                                                               | 0.57     | <i>p</i> > 0.1             |
| Volume total (m <sup>3</sup> ) |               | <b>24</b>      | Total area | 30                      | <b>100</b> | 1                                             | <b><i>p</i> &lt; 0.001</b> | 10                                                              | 0.90     | <b><i>p</i> &lt; 0.001</b> |

Records are assessed as a function of their similarity to the total (24 cores) reconstruction and to the monitored annual discharge. Bold characters indicate cores with a reconstructed frequency of up to 60 % and a reconstructed intensity with *p* values below 0.01

Combination p1: LDB0902, LDB0903, LDB0904 LDB0906, LDB0907, LDB0908

Combination p2: LDBSREF, LDB10P2, LDB1006 LDB1005, LDB1004, LDB10T403 LDB10T402

Combination p3: LDBSREF, LDB10P2, LDB1006 LDB1005, LDB1004, LDB10T403

Combination p4: LDBSREF, LDB10P2, LDB1006 LDB1005, LDB1004

Combination p5: LDBSREF, LDB10P2, LDB1006 LDB1005

Combination p6: LDBSREF, LDB10P2, LDB1006

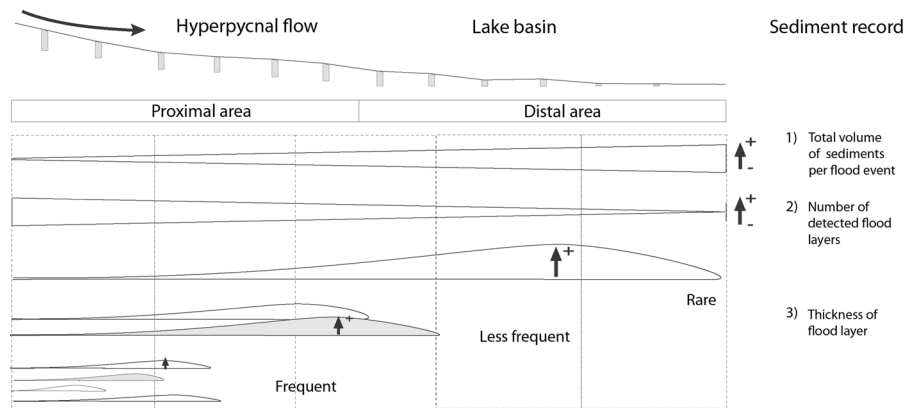


**Fig. 8** Synthetic model of the spatial distribution of flood deposits in Lake Bourget. This theoretical scheme compares the deposition environments of the proximal versus distal area. It shows where and how sediments accumulate by considering

three indicators: 1 the total sediment volumes deposited per event, 2 the number of flood layers recorded by cores and 3 the flood layer thicknesses recorded by cores

events correspond well to the flood record of the last 150 years (Fig. 9a, b). This suggests a threshold in the flood discharge of  $1,500 \text{ m}^3 \text{ s}^{-1}$  for the formation of identifiable flood deposits. Moreover, a significant relationship appeared between discharges and the reconstructed sediment volumes ( $r = 0.90$ ,  $p \leq 0.0001$ ), strongly suggesting that total flood-sediment volumes are related to the maximal annual discharge of flood events. Hence, reconstructed volumes provide a reliable proxy of past flood occurrence and intensity at least over the last 150 years. Nevertheless, human settlements (embankments and dams) could have disrupted the linear relation between discharges and volumes of sediment deposited over the last 350 years (Fig. 9c).

The early 1900s were characterised by the first dam settlements (Fig. 2). The construction of the first hydropower dams around AD 1900 on the Rhône River increased the retention of sediments from the main source contributors (Giuliani et al. 1994; Viollet 2005). However, the strong relation between volumes and monitored annual discharges suggests that the quantity of sediment transported and deposited into Lake Bourget by the Rhône River during flood events has not been significantly affected by the settlements. This might be attributed to the small grain size (mainly clays and fine silts) of the flood sediments brought by the Rhône River into Lake Bourget. These fine particles are mainly in suspension and may thus cross the dams without being deposited. Furthermore, during high-energy flood events, dams generally retain

negligible volumes of water compared with the total transiting volume of water (Doutriaux 2008). However, Genissiat’s dam, built in AD 1948, has the particularity to retain fine sediments (Doutriaux and Couvert 2008), while volumes and monitored annual discharges were compared mostly for events appeared before AD 1948. The only major event recorded by sediments since AD 1948 is the AD 1990 event. It is thus difficult for now to evaluate the consequence of such dams on the volume-to-discharge relation preservation for the more recent period.

#### Flood reconstruction versus historical data (1700s and 1800s)

Historical descriptions were explored to rank the highest past flood events since the mid-1600s. According to our flood record, the four highest volumes of the last 350 years were deposited during the early 1700s, in AD 1686, 1711, 1733, and 1737 (Fig. 9). The highest volume of terrigenous sediments was brought by the AD 1711 event ( $182 \times 10^3 \text{ m}^3$ ), equivalent to more than twice the volume brought by the second most intense flood event ( $81 \times 10^3 \text{ m}^3$  in AD 1733). Only a few descriptions are available for flood events of the upstream Rhône River over the 1700s. Only the AD 1711 flood event was described in detail in the available historic archives because it was remarkably devastating. This event was compared with other higher-energy floods of the 1700s and 1800s to validate the reliability of the reconstructed

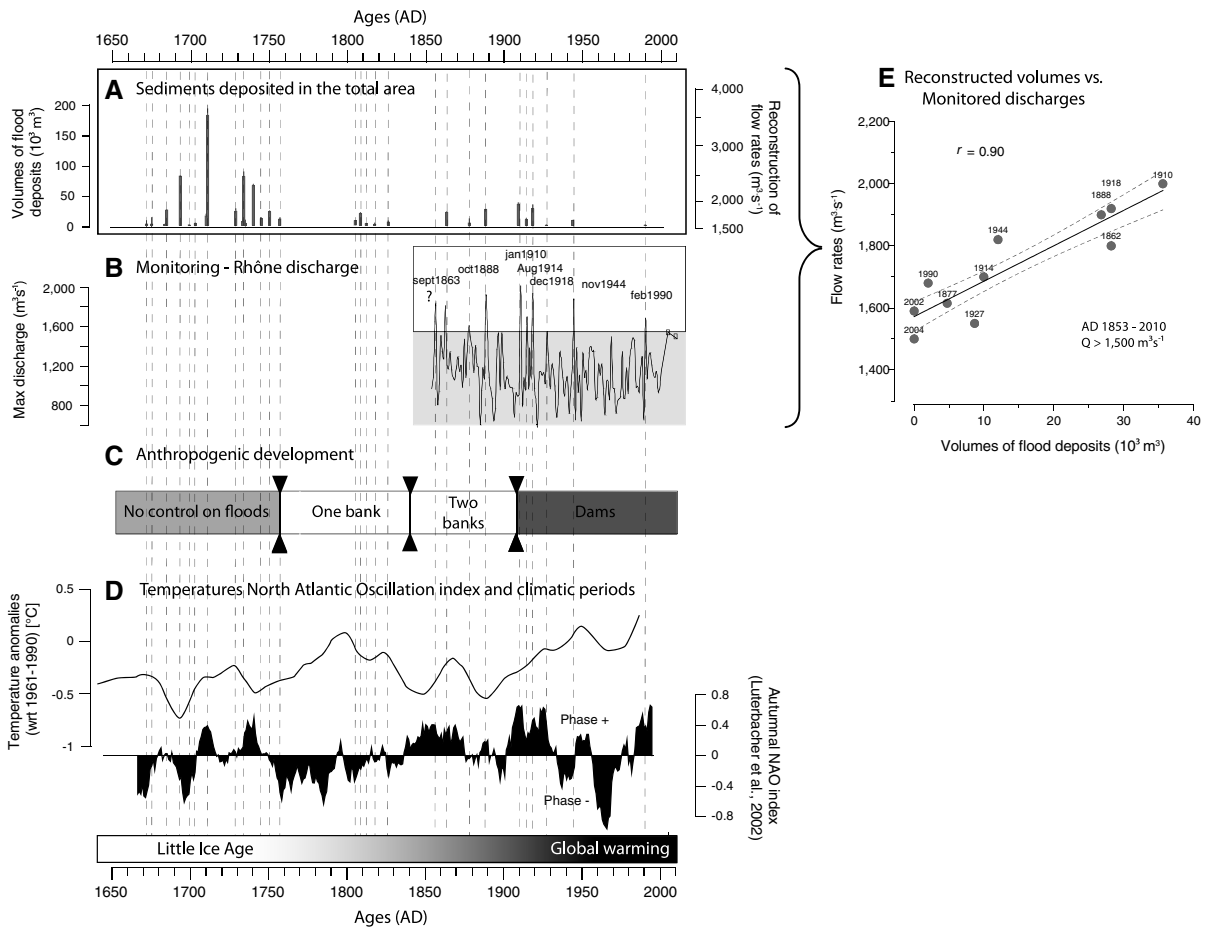


**Fig. 9** **a** Reconstruction of the relative intensity from the total volume calculation compared with **b** the maximum annual discharges of the Rhône River obtained from monitoring data, **c** major anthropogenic development, and **d** temperature (Casty

et al. 2005) and the NAO index (Luterbacher et al. 2002). **e** A cross plot of the reconstructed volumes and monitored discharges reveals a clear linear relationship ( $r = 0.90$ ,  $p = 0.000$ )

flood intensity over historic times. Historical data presented the AD 1711 event as the most important flood event due to the combination of melted snow and generalised extreme precipitation (Champion 1839). This flood event was characterised as exceptional because the level reached “6 feet high of water at the portal of the *Eglise de la Charité*”, in Lyon located 95 km downstream from Lake Bourget (Champion 1839). From AD 1711 to 1839, archives never recorded such a high level of water in Lyon (Champion 1839). This suggests that the AD 1711 flood event was indeed far more intense than other flood events and that relative intensity seems to be preserved through the archives for past events.

Whereas the relative flood intensity seems to be reliably reconstructed over the entire studied period,

we still do not know whether it is preserved continuously between the two periods, i.e., if the single volume-intensity relationship observed over the last 150 years can be extended over the entire studied period. The 1700s and 1800s were affected mainly by embankments that controlled the bed linearity and partly protected the Chautagne swamps from flood hazard. However, those embankments were not continuous, as they still allowed overflow into the Chautagne swamps (Giuliani et al. 1994). Embankments may have prevented only the low-intensity flood events from being recorded. However, the presence of identifiable flood deposits associated with historical events in the early 1800s confirmed that floods could have been recorded after settlements. Hence, the absence of flood deposits for the period

from 1734 to 1841 might more likely be attributed to climate variability than to human embankments.

#### Reconstructed flood activity and possible links to climate changes

Instrumental and historical data show that the flood deposits correspond for 78 % of all cases of autumn and winter flood events triggered by long-lasting and low-intensity rainfalls (type “long-rain flood”; Merz and Blöschl 2003). This is in good agreement with previous observations indicating that these flood events occurred mainly during these two seasons and are associated with oceanic rains (Cholley 1925; Pardé 1928; Chapron et al. 2002). Hence, we assume that our reconstructed flood series represents mostly autumn and winter floods originated from oceanic events linked to the activity of the Westerlies over the last 350 years. A high variability appears in the reconstructed flood activity throughout the studied period. The most significant feature of our flood record is the increase of the flood frequency and intensity over the period AD 1670–1760, which is characterised by long-lasting cold temperatures (Casty et al. 2005; Fig. 9). According to Magny et al. (2003), increased moisture over Western Europe during cooler periods may result from a southward shift and an intensification of the prevailing westerly winds, due to an increase in the thermal gradient between high and low latitudes. Simulations of mid-latitude cyclonic activity and the resulting precipitation patterns provide support for such mechanisms (Bengtsson and Hodges 2006; Raible et al. 2007). In addition, this period of enhanced flood frequency and intensity also corresponds to a well-marked solar minimum, the Maunder minimum (Delaygue and Bard 2011). This may suggest a possible link between solar and flood activities. This relationship was previously proposed based on the reconstructed flood series of Lake Ammersee (Germany), for which the recorded floods are also linked to the variability of the cyclonic activity (Czymzik et al. 2010). Hence, cold temperature and solar minima could enhance the flood activity of large rivers, such as the Rhône River, over the northern flank of the Alps on a multi-decennial timescale. This strongly contrasts with the climate-flood relationships suggested for flash floods, which affect the smaller high-elevation catchments of the region. In the case of flash floods, warming seems indeed to play a dominant role by

favouring the setting of intense convective processes and, in turn, the occurrence of intense mountain-river floods (Wilhelm et al. 2012a, 2013). In contrast, many authors have reported a link between the winter Alpine climate and the North Atlantic Oscillation (NAO) on a sub-decennial timescale. Winters indeed seem moister during positive phases of the NAO (Hurrell 1995; Wanner et al. 1997). This link was investigated herein from the comparison of the reconstructed flood series with the reconstructed index of the NAO (Luterbacher et al. 2002; Fig. 9d). Over the entire studied period, the most intense floods (volumes  $>2 \times 10^3 \text{ m}^3$ ) occurred mostly during the positive phases of the NAO. This suggests that the NAO could also play a dominant role in the generation of intense flood events of large rivers, as suggested by Chapron et al. (2002). Hence, the occurrence of intense flood events of large rivers could be related to complex timescale-dependent interactions between the temperature and the solar activity on a multi-decennial timescale and to the NAO on a sub-decennial timescale.

#### Conclusion

Past flood hazards can be investigated from sediment archives of large plain lakes that develop heterogeneous, meandering deposits. Only the spatial investigation in the Lake Bourget northern area allowed for an accurate reconstruction of the flood intensity and frequency over the last 350 years. In the case of Lake Bourget, the spatial distribution of hyperpycnites depends on the sediment volume brought in the lake during flood events. Large incomes, triggered by high flood events, produce rare thick distal deposits. Lower sediment inputs, triggered by flood events of lower intensity, produce more frequent, but thinner proximal deposits. The use of one isolated core from the distal zone could still provide a reliable chronology of past flood intensity but the chronology would be not complete. For that purpose, the location of the core should be carefully selected. Reconstruction in Lake Bourget suggests that the occurrence of high-energy flood events involving the Rhône River could be related to complex timescale-dependent interactions between the temperature and the solar activity on a multi-decennial timescale and to the NAO on a sub-decennial timescale.

**Acknowledgments** The authors are grateful to Grégoire Ledoux, CEN Université Laval, Québec, for providing the bathymetric map; to Jean-Paul Bravard for helpful suggestions; to Fayçal Soufi, EDYTEM, for help in making the thin sections; and to Cécile Pignol for help in the laboratory. This work was funded by the French National Research Agency (ANR) through research programs “IPER-Rétro” (ANR-08-VUL 005) and “PYGMALION” (ANR-07-BLAN-0133). J.P. Jenny benefited from a PhD joint grant of the ANR Iper-Rétro and from the Assemblée des Pays de Savoie. Bruno Wilhelm benefited from a PhD joint grant of the Communauté de Commune du Grésivaudan and the Assemblée des Pays de Savoie. This research also benefited from a grant from the Laboratory of Excellence (LABEX) ITEM in the framework of the research program “CrHistAl – Crue Historiques dans les Alpes”.

## References

- Allen MR, Ingram WJ (2002) Constraints on future changes in climate and the hydrologic cycle. *Nature* 419(6903):224–232
- Arnaud F, Revel M, Chapron E, Desmet M, Tribouillard N (2005) 7200 years of Rhône river flooding activity in Lake Le Bourget, France: a high-resolution sediment record of NW Alps hydrology. *Holocene* 15:420–428
- Arnaud F, Révillon S, Debret M, Revel M, Chapron E, Jacob J, Giguet-Covex C, Poulenard J, Magny M (2012) Lake Bourget regional erosion patterns reconstruction reveals Holocene NW European Alps soil evolution and paleohydrology. *Quat Sci Rev* 51:81–92
- Bengtsson L, Hodges KI (2006) Storm tracks and climate change. *J Clim* 19:3518–3543
- Bravard JP (1987) Le Rhône du Léman à Lyon. *J Alpine Res* 75:89–91
- Campbell C (1998) Late holocene lake sedimentology and climate change in Southern Alberta, Canada. *Quat Res* 49: 96–101
- Casty C, Wanner H, Luterbacher J, Esper J, Böhm R (2005) Temperature and precipitation variability in the European Alps since 1500. *Int J Climatol* 25:1855–1880
- CEMAGREF (2000) Revisiter la notion de scénario hydrologique de référence pour la caractérisation du risque d’inondation. PhD Thesis, Université Joseph Fourier Grenoble, p 228
- Champion M (1839) Les inondations en France depuis le VI<sup>e</sup> siècle jusqu’à nos jours. V. Dalmont
- Chapron E, Beck C, Pourchet M, Deconinck J (1999) 1822 earthquake-triggered homogenite in Lake Le Bourget (NW Alps). *Terra Nova* 11:86–92
- Chapron E, Desmet M, De Putter T, Loutre MF, Beck C, Deconinck JF (2002) Climatic variability in the northwestern Alps, France, as evidenced by 600 years of terrigenous sedimentation in Lake Le Bourget. *Holocene* 12:177–185
- Chapron E, Arnaud F, Noël H, Revel M, Desmet M, Perdereau L (2005) Rhône River flood deposits in Lake Le Bourget: a proxy for Holocene environmental changes in the NW Alps, France. *Boreas* 34:404–416
- Cholley A (1925) Le régime et les crues du Rhône. *Annales Géographie* 34:454–461
- Christensen JH, Christensen OB (2003) Severe summertime flooding in Europe. *Nature* 421:805–806
- Czymzik M, Dulski P, Plessen B, Grafenstein U von, Naumann R, Brauer A (2010) A 450 year record of spring-summer flood layers in annually laminated sediments from Lake Ammersee (southern Germany). *Water Res* 46:16
- Debret M, Chapron E, Desmet M, Rolland-Revel M, Magand O, Trentesaux A, Bout-Roumazielle V, Nomade J, Arnaud F (2010) North western Alps Holocene paleohydrology recorded by flooding activity in Lake Le Bourget, France. *Quat Sci Rev* 29:2185–2200
- Delaygue G, Bard E (2011) An Antarctic view of Beryllium-10 and solar activity for the past millennium. *Clim Dyn* 36:2201–2218
- Doutriaux E (2008) Est-il possible d’utiliser les ouvrages de la CNR pour abaisser les niveaux d’eau. In: Le Rhône en 100 questions, BRAVARD J.-P., CLEMENS, A., Editors, GRAIE, Villeurbanne, France, pp 52–55
- Doutriaux E, Couvert B (2008) Les sédiments s’accumulent-ils dans les aménagements hydroélectriques du Rhône. In: Le Rhône en 100 questions, BRAVARD J.-P., CLEMENS, A., Editors, GRAIE, Villeurbanne, France, pp 52–55
- Frei C, Schär C (2001) Detection probability of trends in rare events: theory and application to heavy precipitation in the alpine region. *J Clim* 14:1568–1584
- Giguet-Covex C, Arnaud F, Poulenard J, Enters D, Reyss J-L, Millet L, Lazzaroto J, Vidal O (2010) Sedimentological and geochemical records of past trophic state and hypolimnetic anoxia in large, hard-water Lake Bourget, French Alps. *J Paleolimnol* 43:171–190
- Giguet-Covex C, Arnaud F, Enters D, Poulenard J, Millet L, Francus P, David F, Rey P-J, Wilhelm B, Delannoy J-J (2012) Frequency and intensity of high-altitude floods over the last 3.5 ka in northwestern French Alps (Lake Anterne). *Quat Res* 77:12–22
- Gilli A, Anselmetti FS, Ariztegui D, McKenzie JA (2003) A 600-year sedimentary record of flood events from two sub-alpine lakes (Schwendiseen, Northeastern Switzerland). *Eclogae Geol Helv* 96:49–58
- Gilli A, Anselmetti FS, Glur L, Wirth SB (2013) Lake sediments as archives of recurrence rates and intensities of past flood events. In: Schneuwly-Bollschweiler M, Stoffel M, Rudolf-Miklau F (eds) Dating torrential processes on fans and cones. Springer, Netherlands, pp 225–242
- Girardclos S, Baster I, Wildi W, Pugin A, Rachoud-Schneider A-M (2003) Bottom-current and wind-pattern changes as indicated by Late Glacial and Holocene sediments from western Lake Geneva (Switzerland). *Eclog Geol Helvetiae* 96(suppl. 1):39–48
- Giuliani Y, Bravard J-P, Klingeman PC (1994) Morphodynamic impacts on a river affected by a hydro-electric diversion scheme: the Rhône in the Chautagne region of France. *Rev Géogr Lyon* 69:73–87
- Hurrell JW (1995) Decadal trends in the North Atlantic Oscillation: regional temperature and precipitations. *Science* 269:676–679
- Ito T, Iwamoto H, Kamiya K, Fukushima T, Kumon F (2010) Use of flood chronology for detailed environmental analysis: a case study of Lake Kizaki in the northern Japanese Alps, central Japan. *Environ Earth Sci* 60:1607–1618

- Jenny JP, Arnaud F, Dorioz JM, Giguët Covex C, Frossard C, Sabatier P, Millet L, Reyss JL, Tachikawa K, Bard E, Pignol C, Perga ME (2013) A spatiotemporal investigation of varved sediments highlights the dynamics of hypolimnetic hypoxia in a large hard-water lake over the last 150 years. *Limnol Oceanogr* 58(4):1395–1408
- IPCC, Kostaschuck RA, MacDonald GM (2007) (Intergovernmental Panel on Climate Change) (2007) Climate change 2007—the physical science basis. Cambridge University Press, Cambridge
- Lapointe F, Francus P, Lamoureaux SF, Saïd M, Cuven S (2012) 1,750 years of large rainfall events inferred from particle size at East Lake, Cape Bounty, Melville Island, Canada. *J Paleolimnol* 48(1):159–173
- Luterbacher J, Xoplaki E, Dietrich D, Jones PD, Davies TD, Portis D, Gonzalez-Rouco JF, von Storch H, Gyalistras D, Casty C, Wanner H (2002) Extending North Atlantic oscillation reconstructions back to 1500. *Atmos Sci Lett* 2:114–124
- Magny M, Bégeot C, Guiot J, Peyron O (2003) Contrasting patterns of hydrological changes in Europe in response to Holocene climate cooling phases. *Quat Sci Rev* 22:1589–1596
- Merz R, Blöschl G (2003) Regional flood risk—what are the driving processes? *Hydrological Risk, Management and Development*, IAHS Publ 281:49–58
- Mulder T, Chapron E (2011) Flood deposits in continental and marine environments: character and significance. In Slatt RM, Zavala C (eds) *Sediment transfer from shelf to deep water—revisiting the delivery system*. *Am Assoc Petrol Geol* 61:1–30
- Mulder T, Migeon S, Savoye B, Faugères JC (2001) Inversely graded turbidite sequences in the deep Mediterranean: a record of deposits from flood-generated turbidity currents? *Geo-Marine Lett* 21:86–93
- Münich Re Group (2003) Annual review: natural catastrophes 2002. *Münich Re Group*, München, p 62
- Pardé M (1928) Périodicité des grandes inondations et crues exceptionnelles. *J Alpine Res* 16:499–519
- Raible CC, Yoshimori M, Stocker TF, Casty C (2007) Extreme midlatitude cyclones and their implications for precipitation and wind speed extremes in simulations of the Maunder Minimum versus present day conditions. *Clim Dyn* 28:409–423
- Revel-Rolland M, Arnaud F, Chapron E et al (2005) Sr and Nd isotopes as tracers of clastic sources in Lake Le Bourget sediment (NW Alps, France) during the Little Ice Age: palaeohydrology implications. *Chem Geol* 224:183–200
- Schiefer E, Gilbert R, Hassan MA (2011) A lake sediment-based proxy of floods in the Rocky Mountain Front Ranges, Canada. *J Paleolimnol* 45:137–149
- Trenberth KE, Dai A (2007) Effects of Mount Pinatubo volcanic eruption on the hydrological cycle as an analog of geoen지니어링. *Geophys Res Lett* 34(15): Art. No. L15702
- Viollet P-L (2005) Histoire de l'énergie hydraulique: Moulins, pompes, roues et turbines de l'Antiquité au XXe siècle. Presses des Ponts, p 164
- Wanner H, Rickli R, Salvisberg E, Schmutz C, Schiepp M (1997) Global climate change and variability and its influence on alpine climate—concepts and observations. *Theor Appl Clim* 58:221–243
- Wilhelm B, Arnaud F, Enters D, Allignol F, Legaz A, Magand O, Revillon S, Giguët-Covex C, Malet E (2012a) Does global warming favour the occurrence of extreme floods in European Alps? First evidences from a NW Alps proglacial lake sediment record. *Clim Change* 113:563–581
- Wilhelm B, Arnaud F, Sabatier P, Crouzet C, Brisset E, Chaumillon E, Disnar J-R, Guiter F, Malet E, Reyss J-L, Tachikawa K, Bard E, Delannoy J-J (2012b) 1400 years of extreme precipitation patterns over the Mediterranean French Alps and possible forcing mechanisms. *Quat Res* 78:1–12
- Wilhelm B, Arnaud F, Sabatier P, Magand O, Chapron E, Courp T, Tachikawa K, Fanget B, Malet E, Pignol C, Bard E, Delannoy JJ (2013) Palaeoflood activity and climate change over the last 1400 years recorded by lake sediments in the NW European Alps. *J Quat Sci* 28:189–199